

G. F. Van Dusenhausen  
PSol

Analytical Investigation of the Dynamics  
of Tethered Constellations in Earth Orbit (Phase II)

Contract NAS8-36606

Quarterly Report # 2

For the period 22 June 1985 through 21 September 1985

Principal Investigator

Dr. Enrico Lorenzini

October 1985

Prepared for  
National Aeronautics and Space Administration  
Marshall Space Flight Center, Alabama 35812

Smithsonian Institution  
Astrophysical Observatory  
Cambridge, Massachusetts 02138

The Smithsonian Astrophysical Observatory  
is a member of the  
Harvard-Smithsonian Center for Astrophysics



N86-19336

Unclas  
G3/13 16332

(NASA-CR-178607) ANALYTICAL INVESTIGATION  
OF THE DYNAMICS OF TETHERED CONSTELLATIONS  
IN EARTH ORBIT (PHASE 2) Quarterly Report,  
22 Jun. - 21 Sep. 1985 (Smithsonian  
Astrophysical Observatory) 36 p

Analytical Investigation of the Dynamics  
of Tethered Constellations in Earth Orbit (Phase II)

Contract NAS8-36606

Quarterly Report # 2

For the period 22 June 1985 through 21 September 1985

Principal Investigator  
Dr. Enrico Lorenzini

Co-Investigators  
Mr. David A. Arnold  
Dr. Mario D. Grossi  
Dr. Gordon E. Gullahorn

October 1985

Prepared for  
National Aeronautics and Space Administration  
Marshall Space Flight Center, Alabama 35812

Smithsonian Institution  
Astrophysical Observatory  
Cambridge, Massachusetts 02138

The Smithsonian Astrophysical Observatory  
is a member of the  
Harvard-Smithsonian Center for Astrophysics

CONTENTS

	Page
<b>Abstract</b> . . . . .	3
<b>Figure Captions</b> . . . . .	4
<b>SECTION 1.0 INTRODUCTION</b> . . . . .	5
<b>2.0 TECHNICAL ACTIVITY DURING REPORTING PERIOD AND PROGRAM STATUS</b> . . . . .	6
<b>2.1 Introductory Remarks</b> . . . . .	6
<b>2.2 Updated Mathematical Model With Elastic Tethers And Longitudinal Dampers</b> . . . . .	7
<b>2.3 General Considerations Regarding The Damping Of Attitude Librations And Transverse Oscillations</b> . . . . .	11
<b>2.4 Selection Of The Control Parameters</b> . . . . .	14
<b>2.5 New Deployment Control Law</b> . . . . .	17
<b>2.6 Computer Simulation Of The Deployment Phase</b> . . . . .	19
<b>2.7 Computer Simulation Of The Station-Keeping Phase</b> . . . . .	28
<b>2.8 Concluding Remarks</b> . . . . .	34
<b>3.0 PROBLEMS ENCOUNTERED DURING REPORTING PERIOD</b> . . . . .	34
<b>4.0 ACTIVITY PLANNED FOR THE NEXT REPORTING PERIOD</b> . . . . .	35

**Abstract**

This Quarterly Report analyzes the deployment maneuver of three-axis vertical constellations with elastic tethers. The deployment strategy devised in Quarterly Report #1 has been improved. Dampers have been added to the system. Effective algorithms for damping out the fundamental vibrational modes of the system have been implemented. This Quarterly Report also shows simulations of a complete deployment and a subsequent station keeping phase of a three-mass constellation.

**PRECEDING PAGE BLANK NOT FILMED**

Figure Captions

Figure 2.2.1 - Geometry and Lagrangian Coordinates for a Three-Mass Constellation

Figure 2.2.2 - Schematic Model of the Longitudinal Damper

Figure 2.3.1 - Schematic Model of the Rotational/Transverse Damper

Figure 2.6.1 - Dynamic Response of a Three-Mass Constellation During  
(a) - (n) Deployment

Figure 2.7.1 - Dynamic Response of a Three-Mass Constellation During  
(a) - (1) Station-Keeping

## 1.0 INTRODUCTION

This is the second Quarterly Report submitted by SAO under contract NAS8-36606, "Analytical Investigation of the Dynamics of Tethered Constellations in Earth Orbit (Phase II)," Dr. Enrico Lorenzini, PI, and covers the period from 22 June 1985 through 21 September 1985.

## 2.0 TECHNICAL ACTIVITY DURING REPORTING PERIOD AND PROGRAM STATUS

### 2.1 Introductory Remarks

The two-dimensional equations of motion for three-mass constellations were derived in Quarterly Report #1. In that Quarterly Report, however, the two tethers connecting the three masses were assumed to be unstretchable. The control law used for deployment was a rate control law without angular feedbacks. The deployment maneuver was fast but the control law was unable to damp out completely the attitude and transverse oscillations of the constellation. This time, on the contrary, the two tethers are assumed to be elastic with generic characteristics. The right hand terms of the equations of motion developed in Quarterly Report #1 are therefore transformed as shown in the following sections.

Two longitudinal dampers, aligned with the two tethers, have been added to the system. Angular feedbacks have been implemented in the rate control law in order to damp out the attitude and transverse vibrations of the constellations. The following sections deal with the incorporation of the above mentioned additional features into the mathematical model. The appropriate control parameters are then selected and simulations of a deployment and a station-keeping phase are performed.

## 2.2 Updated Mathematical Model With Elastic Tethers And Longitudinal Dampers

The two-dimensional equations of motion (2.2.15) in Quarterly Report #1 were derived under the general assumption that the three masses were generically located in the orbital plane. The only assumption regarding internal forces was that a force (tension)  $T_1$  was exchanged between masses  $m_1$  and  $m_2$  and a similar force (tension)  $T_3$  was exchanged between masses  $m_2$  and  $m_3$ . In the above-mentioned Quarterly Report the tethers were assumed to be unstretchable and the tether tensions were therefore derived by solving the related equations of motion for given values of the parameters on the left hand side of the equations. By assuming the tethers to be elastic, the tether tension is computed by the elastic stretch times the tether stiffnesses as follows:

$$T_1 = \frac{E_1 A_1}{\ell_1} (\ell_1 - \ell_{o1})$$

$$T_3 = \frac{E_3 A_3}{\ell_3} (\ell_3 - \ell_{o3}) \quad (2.2.1)$$

In equations (2.2.1), referring to tether #1 and tether #2 as shown in Figure 2.2.1,  $E$  is the elastic modulus of the tether material,  $A$  is the tether cross section,  $\ell$  is the actual tether length and  $\ell_o$  is the natural tether length. Note that all the quantities referred to tether #2 have the subscript 3 for consistency of notation.

Two longitudinal oscillation dampers (one per tether) have been also added to the system in order to damp out the elastic longitudinal oscillations of the two tethers. In this model the longitudinal dampers are assumed to be two classical spring-dashpot systems with a length gain  $K_d$  and a velocity gain  $K_v$ . We can therefore write:

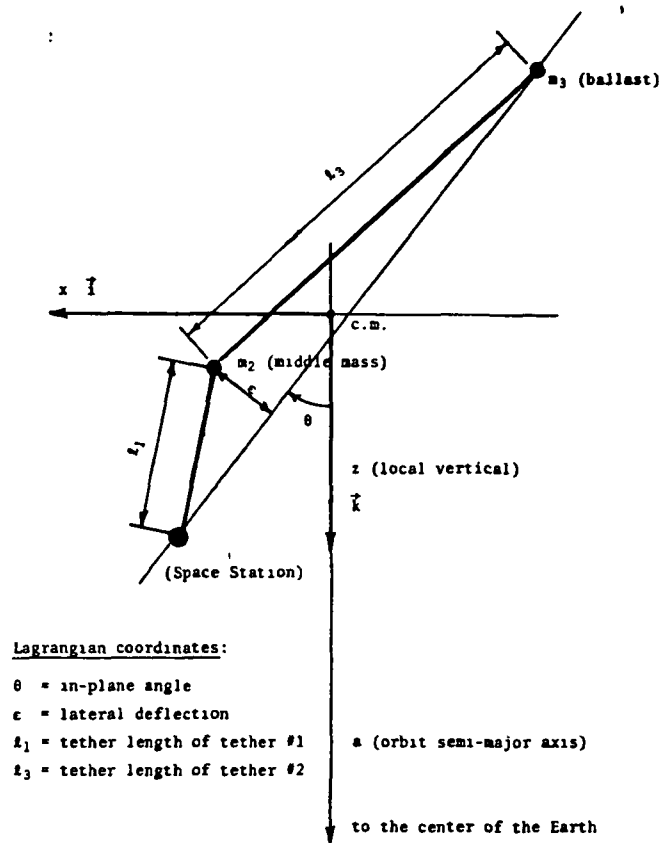


Figure 2.2.1

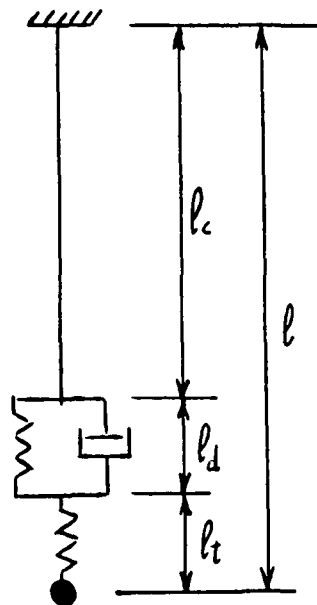


Figure 2.2.2

$$T_1 = K_{d1}l_{d1} + K_{\dot{d}1}\dot{l}_{d1}$$

$$T_3 = K_{d3}l_{d3} + K_{\dot{d}3}\dot{l}_{d3} \quad (2.2.2)$$

The tethers' tensions, according to equations (2.2.1), and taking into account the lengths of the longitudinal dampers, are also given by:

$$T_1 = \frac{E_1A_1}{l_1} (l_1 - l_{d1} - l_{c1}) = K_{t1}l_{t1}$$

$$T_3 = \frac{E_3A_3}{l_3} (l_3 - l_{d3} - l_{c3}) = K_{t3}l_{t3} \quad (2.2.3)$$

where  $E_1A_1/l_1 = K_{t1}$  and  $E_3A_3/l_3 = K_{t3}$  are the tethers' stiffnesses and  $l_{t1}$ ,  $l_{t3}$  are the elastic stretches of the respective tethers.

By combining equations (2.2.2) and (2.2.3) we finally get the expressions for  $\dot{l}_{d1}$  and  $\dot{l}_{d3}$  as follows:

$$\dot{l}_{d1} = \frac{K_{t1}}{K_{d1}} (l_1 - l_{d1} - l_{c1}) - \frac{K_{d1}}{K_{d1}} l_{d1}$$

$$\dot{l}_{d3} = \frac{K_{t3}}{K_{d3}} (l_3 - l_{d3} - l_{c3}) - \frac{K_{d3}}{K_{d3}} l_{d3} \quad (2.2.4)$$

Equations (2.2.3) and equations (2.2.4) should be added to equations (2.2.15) of Quarterly Report #1 in order to get the complete set of equations of motion for the system with elastic tethers and longitudinal dampers. The second order derivatives  $\ddot{l}_1$  and  $\ddot{l}_3$  must be expressed explicitly in the last two equations of motion in order to make them suitable for numerical integration. If we define  $\gamma = R_3l_3 - R_1l_1$  so that  $\dot{\gamma} = R_3\dot{l}_3 - R_1\dot{l}_1$  (in order to shorten the notation) the final equations are as follows

$$T_1 = K_{t1} (\ell_1 - \ell_{d1} - \ell_{c1})$$

$$T_3 = K_{t3} (\ell_3 - \ell_{d3} - \ell_{c3})$$

$$\dot{\ell}_{d1} = \frac{K_{t1}}{K_{d1}} (\ell_1 - \ell_{d1} - \ell_{c1}) - \frac{K_{d1}}{K_{d1}} \ell_{d1}$$

$$\dot{\ell}_{d3} = \frac{K_{t3}}{K_{d3}} (\ell_3 - \ell_{d3} - \ell_{c3}) - \frac{K_{d3}}{K_{d3}} \ell_{d3} \quad (2.2.5)$$

$$\begin{aligned} \ddot{\theta} = & -1 / \left[ m_1 (\dot{\ell}_1^2 + \gamma \dot{\ell}_1) + m_3 (\dot{\ell}_3^2 - \gamma \dot{\ell}_3) + R_2 (m_1 + m_3) \epsilon^2 \right] \cdot \\ & \left\{ m_1 \left[ 2\ell_1 (\dot{\theta} - \Omega) (\dot{\ell}_1 + \dot{\gamma}) + 3\Omega^2 \ell_1 \cos \theta \sin \theta (\ell_1 + 2\gamma) - 3\Omega^2 \ell_1 R_2 \epsilon \cos (2\theta) \right] + \right. \\ & m_3 \left[ 2\ell_3 (\dot{\theta} - \Omega) (\dot{\ell}_3 + \dot{\gamma}) + 3\Omega^2 \ell_3 \cos \theta \sin \theta (\ell_3 + 2\gamma) + 3\Omega^2 \ell_3 R_2 \epsilon \cos (2\theta) \right] + \\ & \left. R_2 (m_1 + m_3) \left[ 2\epsilon \dot{\ell} (\dot{\theta} - \Omega) - 3\Omega^2 \epsilon^2 \cos \theta \sin \theta \right] \right\} \end{aligned}$$

$$\begin{aligned} \ddot{\epsilon} = & \left[ \epsilon (\dot{\theta} - \Omega)^2 + 3\Omega^2 \epsilon \sin^2 \theta \right] + m_{tot} / (m_1 + m_3) \cdot (2\Omega \dot{\gamma} - 3\Omega^2 \gamma \cos \theta \sin \theta) - \\ & \epsilon (T_1 / \ell_1 + T_3 / \ell_3) / \left[ R_2 (m_1 + m_3) \right] \end{aligned}$$

$$\ddot{\ell}_1 = (b_1 a_{22} - b_2 a_{12}) / (a_{11} a_{22} - a_{12} a_{21})$$

$$\ddot{\ell}_2 = (b_2 a_{11} - b_1 a_{21}) / (a_{11} a_{22} - a_{12} a_{21})$$

where:

$$a_{11} = m_1 (1 - R_1)$$

$$a_{12} = m_1 R_3$$

$$a_{21} = m_3 R_1$$

$$a_{22} = m_3 (1 - R_3) \quad (2.2.6)$$

$$b_1 = m_1 \left[ \Omega^2 (3 \cos^2 \theta - 1) (\ell_1 + 2\gamma) + (\dot{\theta} - \Omega)^2 (\ell_1 + \gamma) + \right. \\ \left. 3\Omega^2 R_2 \epsilon \cos \theta \sin \theta + 2\Omega R_2 \dot{\ell} \right] + T_1$$

$$b_2 = m_3 \left[ \Omega^2 (3 \cos^2 \theta - 1) (\ell_3 - 2\gamma) + (\dot{\theta} - \Omega)^2 (\ell_3 + \gamma) - \right. \\ \left. 3\Omega^2 R_2 \epsilon \cos \theta \sin \theta - 2\Omega R_2 \dot{\ell} \right] + T_3$$

Equations (2.2.5) together with (2.2.6), and with a suitable expression for the tether commanded lengths  $l_{c1}$  and  $l_{c3}$ , are the complete mathematical model of the system under investigation. Suitable control algorithms will be developed in the next subsections.

### 2.3 General Considerations Regarding The Damping Of Attitude Librations And Transverse Oscillations

The overall attitude motion of a three-mass system with the middle mass at the system c.m. can be well approximated by the two-mass system's equations of motion. For the purpose of deriving a tether control algorithm for damping out the attitude librations, the above mentioned approximation is more than satisfactory. The simplified and linearized equation of motion for in-plane attitude oscillations is as follows:

$$\ddot{\theta} l^2 - 2(\dot{\theta} - \Omega) \dot{l} l + 3\Omega^2 l^2 \theta = 0 \quad (2.3.1)$$

In equation (2.3.1) the second term is the dissipative one. Therefore the energy dissipated per each libration cycle is given by:

$$E_d = 2 \int_0^{\tau} \dot{l} l (\dot{\theta} - \Omega) \dot{\theta} dt \quad (2.3.2)$$

where  $\tau$  is the period of the in-plane libration. Our goal is to implement a tether control law that makes  $E_d \gg 0$ .

If we consider that  $\dot{\theta}$  is cosinusoidal (with the assumption of  $t = 0$  when  $\theta = 0$ ) and that  $\Omega$  is constant, a good tether control law appears to be:

$$l = l_0 (1 - K_\theta \theta) \quad (2.3.3)$$

where the gain  $K_\theta$  must be greater than zero and  $l_0$  is the tether length for  $\theta = 0$ . It is important to note that the implementation of the control law (2.3.3) assumes that the value of the angle  $\theta$  is provided to the reeling systems of the constellation. If we now substitute (2.3.3) into (2.3.2), omitting the second order terms, we get:

$$E_d \simeq 2l_0^2 K_\theta \left( \int_0^r \dot{\theta}^2 \Omega dt - \int_0^r \dot{\theta}^3 dt \right) \quad (2.3.4)$$

In equation (2.3.4) the dominating term is the first integral under parenthesis while the second integral is negligible. The orbital rate, therefore, strongly influences the damping of the in-plane librations. It is interesting to note that the trajectory followed by the end masses in a damping cycle is not an eight-shaped yo-yo cycle but an S-shaped cycle. In other words the tether is shortened during the retrograde part of the libration and is lengthened during the prograde part as shown in Figure 2.3.1. The control law expressed by equation (2.3.3) can also effectively damp the transverse vibrations of the middle mass (coordinate  $\epsilon$  in Figure 2.3.1) by modifying the previous control law for the two tethers as follows:

$$\begin{aligned} l_1 &= l_{01} (1 - K_\theta \theta - K_\epsilon \epsilon / l_1) \\ l_3 &= l_{03} (1 - K_\theta \theta + K_\epsilon \epsilon / l_3) \end{aligned} \quad (2.3.5)$$

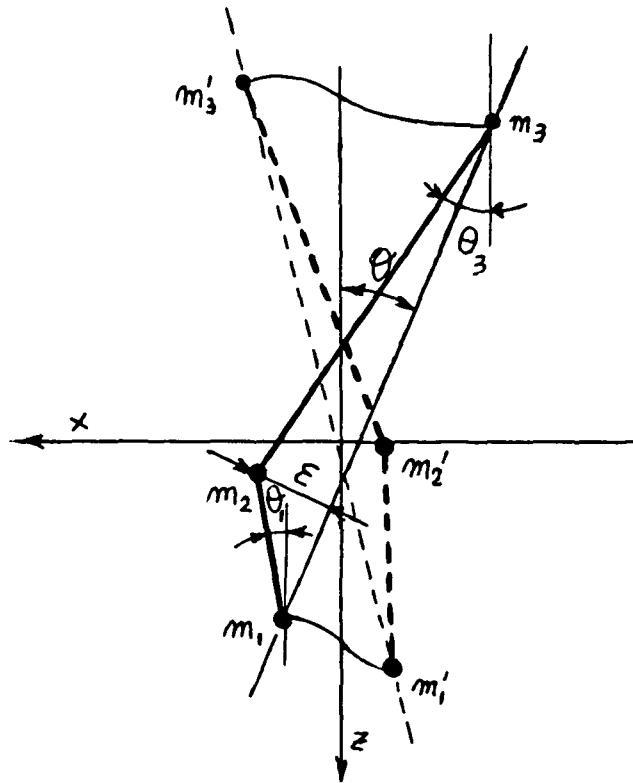


Figure 2.3.1

The tether control law, therefore, is sensitive both to the overall attitude of the constellation ( $\theta$ ) and to the transverse displacement of the middle mass ( $\epsilon$ ). A simplified version of (2.3.5) can be obtained by assuming  $K_\epsilon = K_\theta$  so that, with reference to Figure 2.3.1, we get:

$$\begin{aligned} \ell_1 &= \ell_{o1} [1 - K_\theta(\theta + \epsilon/\ell_1)] = \ell_{o1} (1 - K_\theta\theta_1) \\ \ell_3 &= \ell_{o3} [1 - K_\theta(\theta - \epsilon/\ell_3)] = \ell_{o3} (1 - K_\theta\theta_3) \end{aligned} \quad (2.3.6)$$

This simplified version, where knowledge of the values of angles  $\theta_1$  and  $\theta_3$  is required, is the one adopted in the following simulations.

#### 2.4 Selection Of The Control Parameters

In subsection 2.2 we derived the analytical expression of a control law potentially effective in damping out the in-plane oscillations and the transverse oscillations of the system. In subsection 2.3 we also dealt with the addition of passive longitudinal dampers to the system. In this subsection we shall preliminarily compute the values of the gains (control parameters) in the damping active control laws and in the passive longitudinal dampers.

In order to maximize the energy transfer between the tethers' longitudinal vibrations and the respective longitudinal passive dampers' oscillations the natural frequency of each damper should be equal to the natural frequency of the associated tether. Unfortunately the tethers' frequencies change during deployment because the tethers' lengths change. Since a passive damper is not capable of variable tuning, it must be designed for specific tuning. By actively damp-

ing longitudinal oscillations by means of reel-control this problem is overcome at the expense of further sophistication of the system. This possibility has not been eliminated and will be explored in the follow-up to this study.

Each passive damper has been tuned to the frequency of the associated tether at the tether length pertaining to the station-keeping phase. In this way the most effective damping of longitudinal vibrations is obtained during station-keeping while the damping performance is degraded during deployment. The stiffnesses of tether #1 and tether #2 for two millimeter diameter kevlar tethers and fully deployed tether lengths are:

$$\begin{aligned} K_{t1} &= E_1 A_1 / \ell_{1sk} = 67.81 \text{ N/m} \\ K_{t3} &= E_3 A_3 / \ell_{3sk} = 6.781 \text{ N/m} \end{aligned} \quad (2.4.1)$$

In order to tune the longitudinal dampers we must select the dampers' stiffnesses in equations (2.2.2) as follows:

$$\begin{aligned} K_{d1} &= K_{t1} \\ K_{d3} &= K_{t3} \end{aligned} \quad (2.4.2)$$

The spring-mass mode longitudinal oscillation frequencies for the constellation under investigation in the fully deployed configuration are:

$$\begin{aligned} \omega_{t1} &= \sqrt{E_1 A_1 / (\ell_{1sk} m_1)} = 2.735 \times 10^{-2} \text{ rad/sec} \\ \omega_{t3} &= \sqrt{E_3 A_3 / (\ell_{3sk} m_3)} = 2.735 \times 10^{-2} \text{ rad/sec} \end{aligned} \quad (2.4.3)$$

Some test simulations have been performed in order to identify good damping coefficients in equations (2.2.2). By increasing the damping coefficients the dampers proved to be more effective. An adimensional coefficient  $\xi = 0.9$  was adopted for both longitudinal dampers although the dynamic response for supercritical damping coefficients has not been explored yet. Consequently the dimensional damping coefficients are as follows:

$$K_{d1} = 2\xi\omega_{\ell 1}m_1 = 4460.24 \text{ N/m/sec}$$

$$K_{d3} = 2\xi\omega_{\ell 3}m_3 = 446.024 \text{ N/m/sec} \quad (2.4.4)$$

The selection of the gains (equations 2.3.6) for the rotational/transverse oscillations dampers (active damping system) has been made on a trial and error basis. The major constraint is the tether length variation over a damping cycle. The maximum tether length variation was finally selected as 1% of the fully deployed tether length per degree of system's libration. The gain in equations (2.3.6) is therefore:

$$K_{\theta} = 0.55 \quad (2.4.5)$$

By adopting the above mentioned value the damping of the constellation's librations is very good. A more than satisfactory damping of the system's transverse oscillations is also achieved. The transverse oscillations' damping can be further improved by using equations (2.3.5) instead of (2.3.6), namely by adopting different values for the gains  $K_{\theta}$  and  $K_{\ell}$ . This option, however, has not been explored yet. Results of the simulation runs performed will be illustrated in subsections 2.6 and 2.7.

## 2.5 New Deployment Control Law

The tether rate control law adopted in the deployment simulations of Quarterly Report #1 has been modified as follows. The initial part of the deployment is still an exponentially accelerated phase followed by an exponentially decelerated phase with continuous tether speed at the transition between the two phases. In formulae we can write:

Phase I (acceleration)

$$l_{1c} = l_{1I} e^{\alpha t} \quad \text{if } l_{1I} < l_{1c} \leq l_{1T} \quad (2.5.1)$$

$$l_{3c} = l_{3I} e^{\alpha t} \quad \text{simultaneous transition for the two tethers}$$

Phase II (deceleration)

$$l_{1c} = (l_{1T} - l_{1I})e^{-\beta t} + l_{1I} \quad \text{if } l_{1c} > l_{1T}$$

$$l_{3c} = (l_{3T} - l_{3I})e^{-\beta t} + l_{3I} \quad (2.5.2)$$

where  $\beta = \alpha / (l_{1I} / l_{1T} - 1.)$  and  $\alpha = \frac{3}{4} \Omega \sin(2\theta_c)$ .

All the characteristic tether lengths pertaining to tether #1 and tether #2, in formulae (2.5.1) and (2.5.2), are in the ratio  $l_{1sk} / l_{3sk}$ . The angle  $\theta_c$  is the constant in-plane angle assumed by the constellation during the acceleration phase. In the deployment control law the deceleration phase does not make the tether velocity approach zero. The tethers' controllers simultaneously activate the rotational damper when the tether speed in each tether, during the deceleration

ating phase, is equal (or very close) to the tether speed required by the rotational damper for that tether length and that libration angle. The equality of the tether speeds, however, does not guarantee that the tether lengths, required by the two different control laws, match. For this reason provisions must be made for providing a smooth transition. Appropriate values of  $\theta_c$  and of the transition length  $l_{1T}$  must be adopted in order to reduce the tether length mismatch at the transition. In addition a transition control law must be devised in order to compensate for the residual tether length mismatch. The transition control law must be devised in such a way that its initial and final velocity are zero. Therefore a semi-cycle of a cosinusoidal law has been adopted. All the above mentioned considerations can be translated into formulae as follows (similar formulae apply to tether #2):

$$\text{If: } [\dot{l}_{1c}]_{\text{acc.phase}} \simeq [\dot{l}_{1c}]_{\text{rot.damp.on}} \text{ that implies } -\beta(l_{1c} - l_{1t}) \simeq l_{1sk}K\theta\dot{\theta}$$

then:

$$l_{1c} = l_{1sk} (1 - f_{tr} - K\theta) \quad (2.5.3)$$

$$f_{tr} = f_{otr} \cos\left(\frac{\pi}{2} \frac{t}{\Delta t}\right) \quad (2.5.4)$$

and:

$$f_{otr} = (l_{1c \text{ rot damp.on}} - l_{1c \text{ acc.phase}}) / l_{1sk}$$

In equation (2.5.4)  $\Delta T$  is the transition time.

The control parameters which proved to provide a good dynamic response for the deployment maneuver are as follows:

$$\begin{aligned}l_{1T} &= 500 \text{ m} \\ \theta_c &= 30^\circ \\ \Delta T &= 2000 \text{ sec}\end{aligned}\tag{2.5.5}$$

A detailed description of the deployment maneuver obtained by using the above mentioned control law and control parameters is given in the next subsection.

## 2.6 Computer Simulation Of The Deployment Phase

Several simulation runs of the deployment maneuver have been performed in order to select the appropriate control parameters previously described in subsections 2.4 and 2.5. In this subsection the dynamic response of the system during deployment is shown for that "best" selection of parameters. The deployment maneuver was started from initial tethers' lengths of  $l_{1T} = 20 \text{ m}$  and  $l_{3T} = 200 \text{ m}$ . The system with elastic tether shows a strong tendency to go slack in the very beginning of the deployment maneuver. Any small initial mismatch may cause a temporary slack tether condition. An in-line thruster and an appropriately tuned longitudinal damper can help considerably in relieving the slack tether tendency. A detailed analysis of the initial deployment phase should follow the present study of the deployment maneuver. This type of analysis has been postponed, however, for follow-up studies of the three-mass constellations. Figure 2.6.1 from (a) to (n) shows the dynamic response during deployment with longitudinal dampers tuned to the station-keeping tether lengths and rotational/transverse dampers activated as described in the previous subsection.

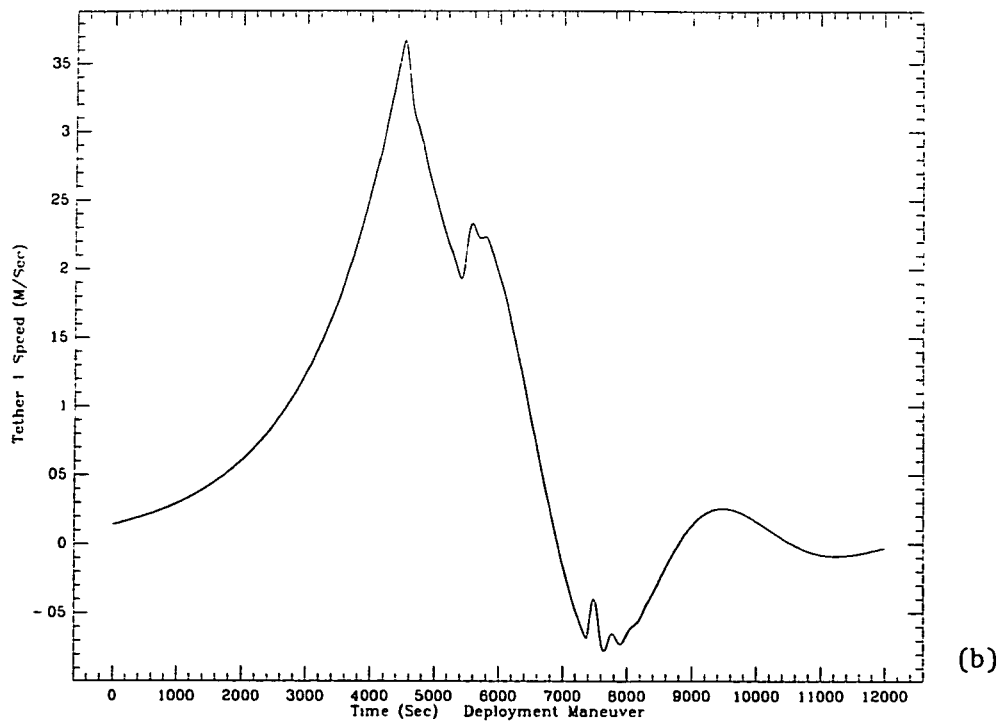
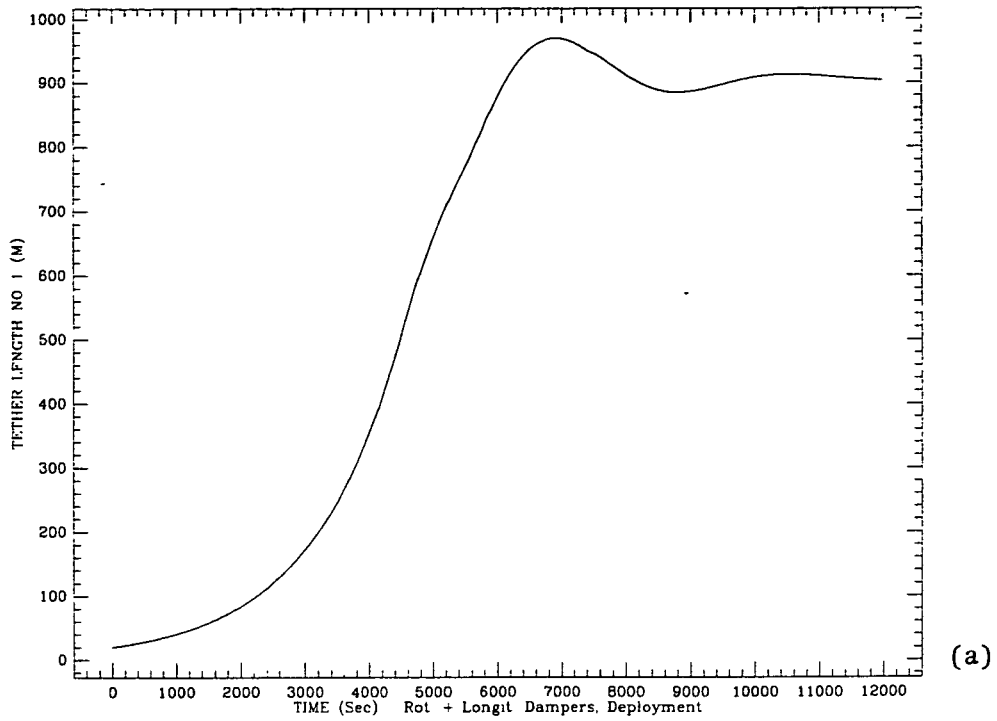
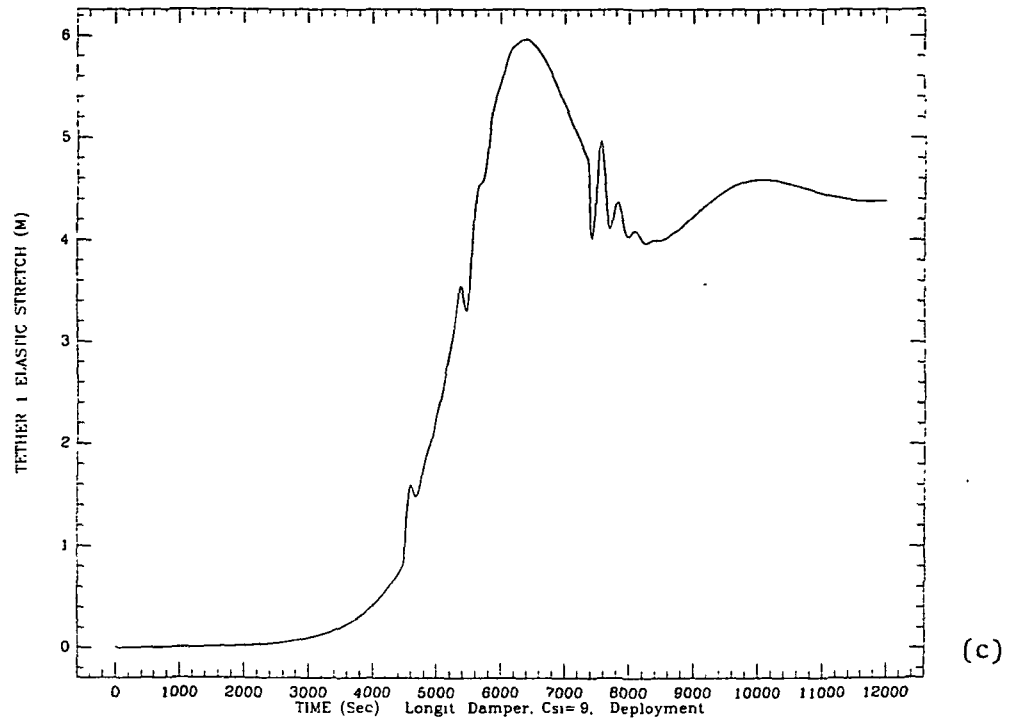
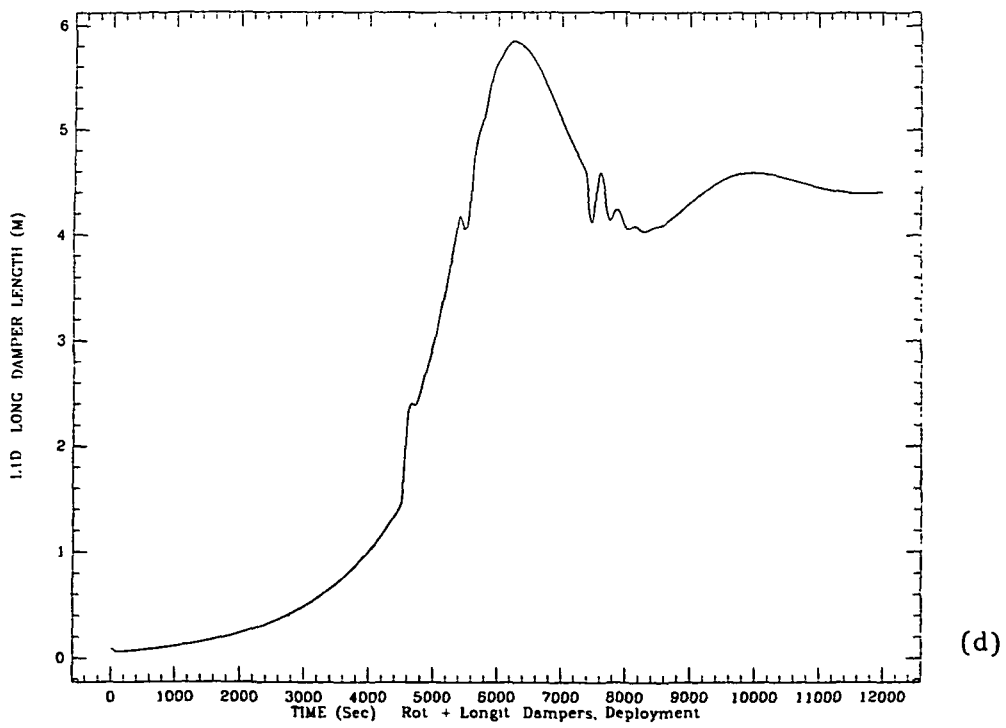


Figure 2.6.1 (a) and (b)



(c)



(d)

Figure 2.6.1 (c) and (d)

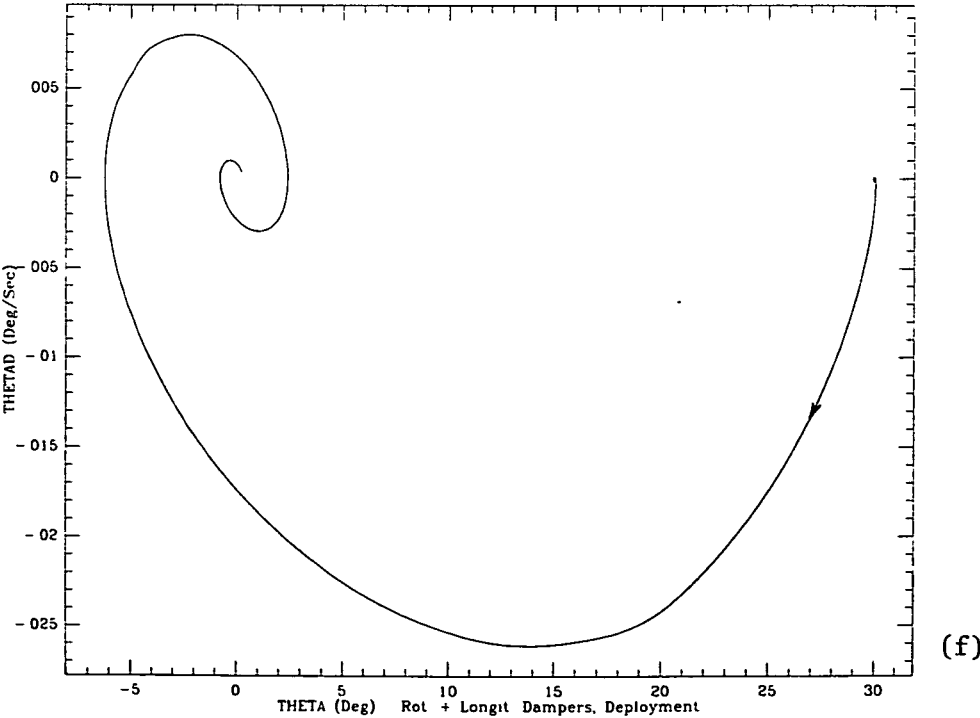
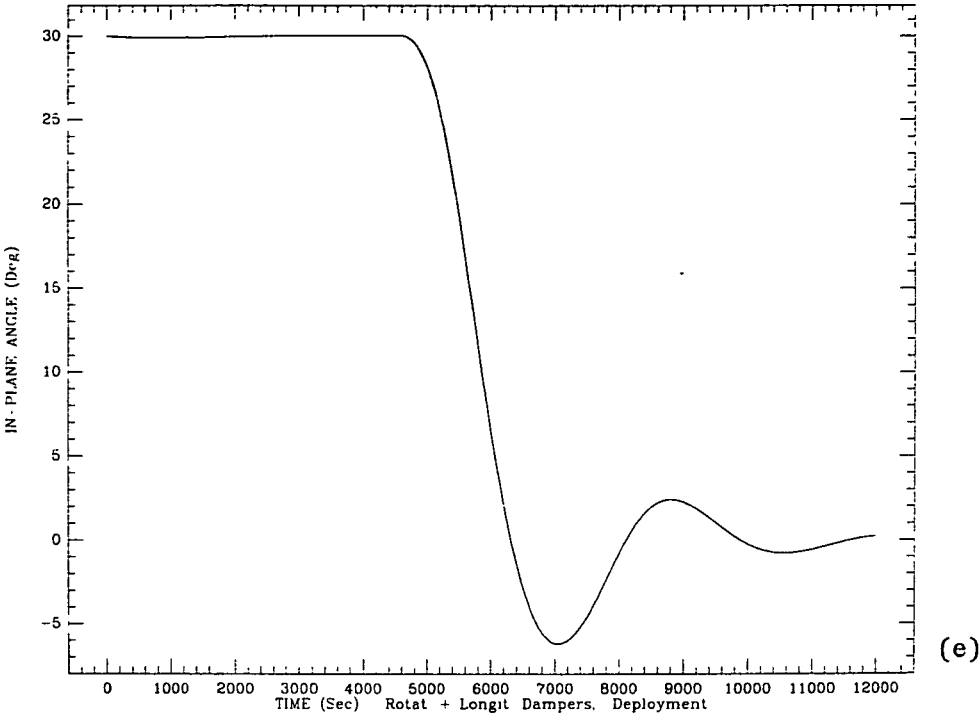


Figure 2.6.1 (e) and (f)

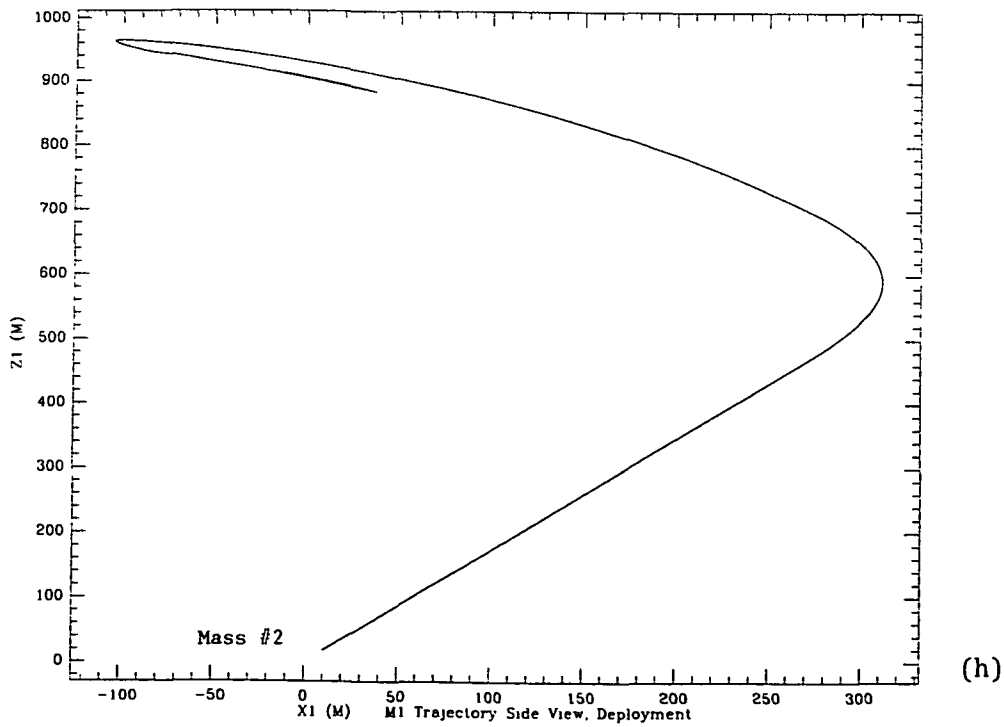
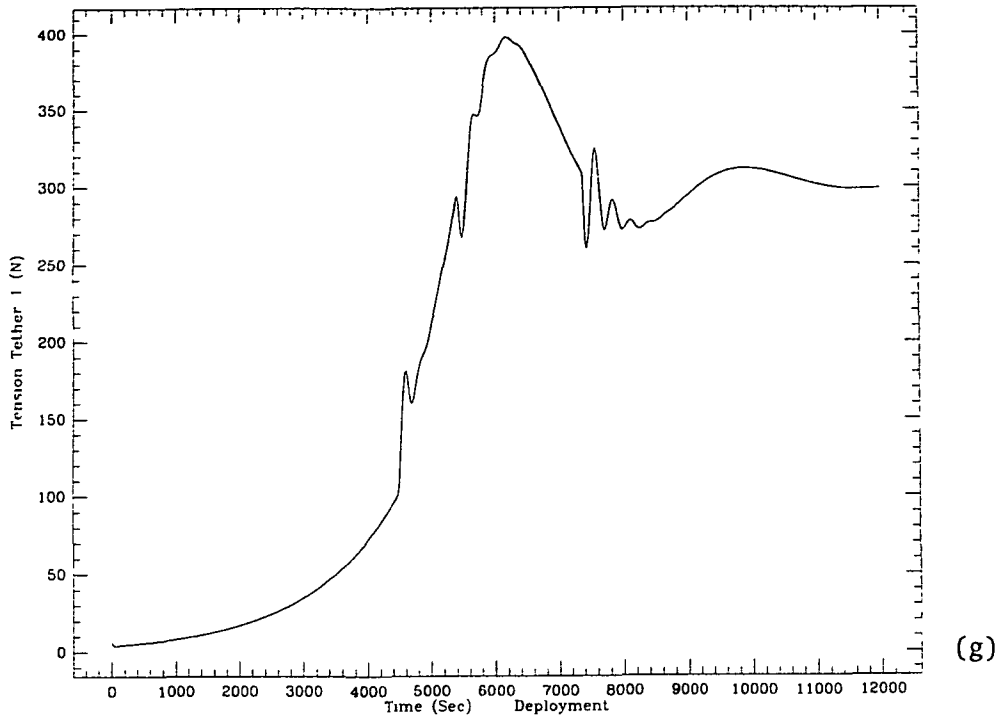


Figure 2.6.1 (g) and (h)

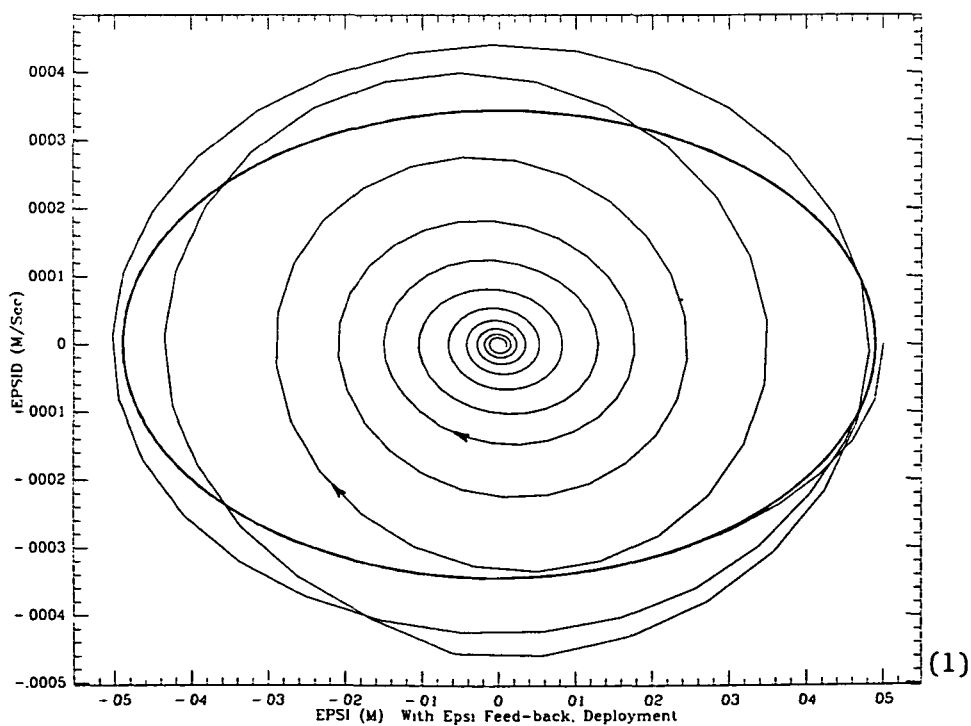
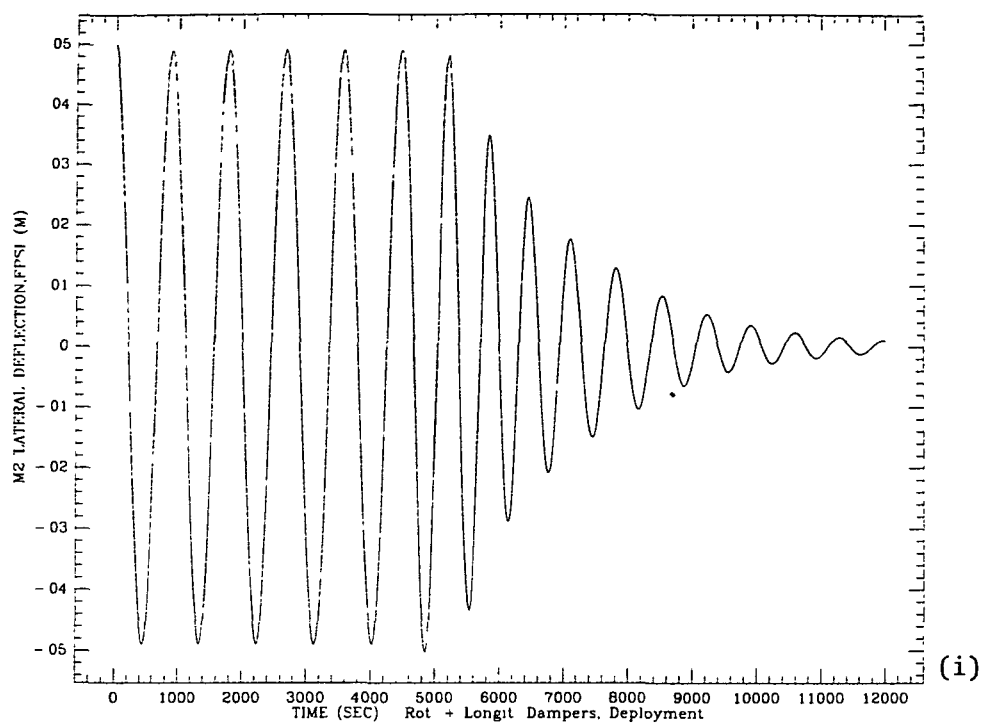


Figure 2.6.1 (i) and (1)

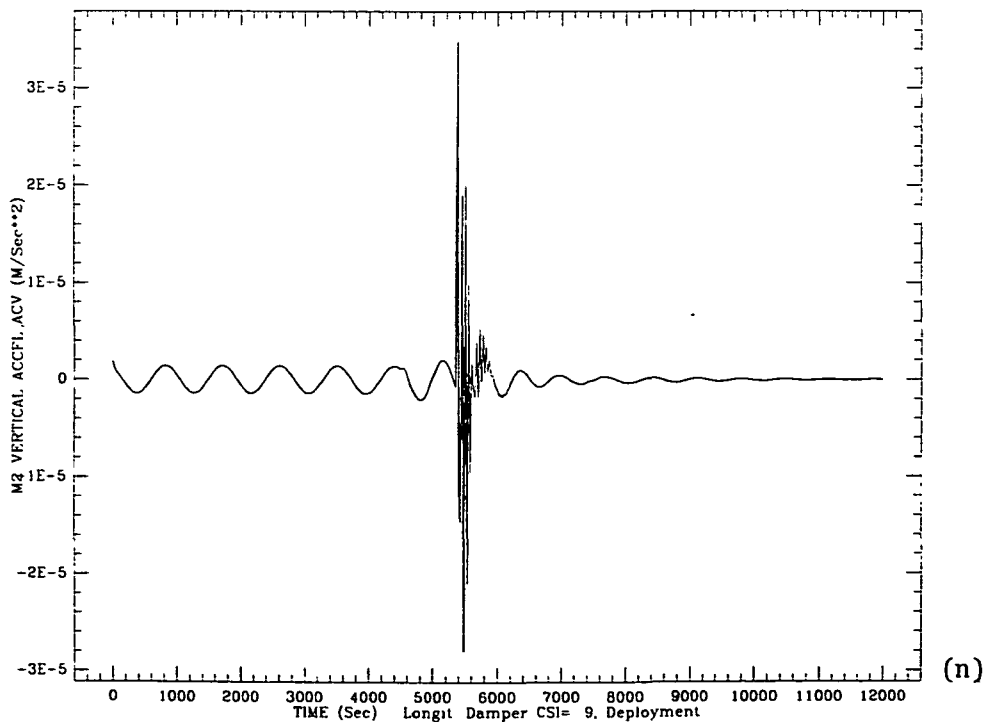
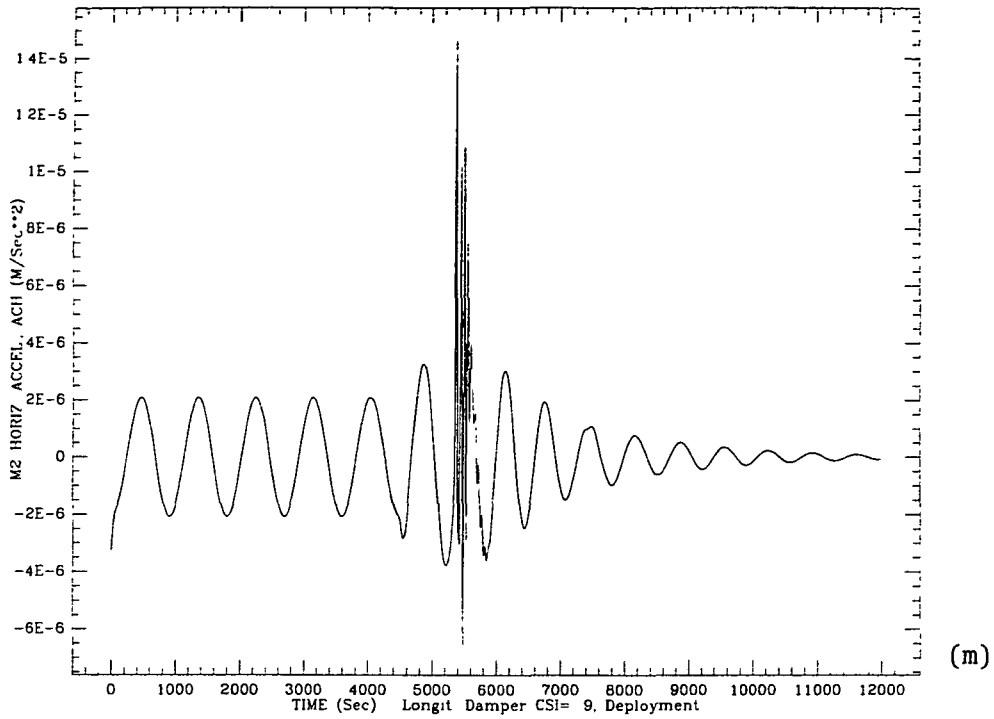


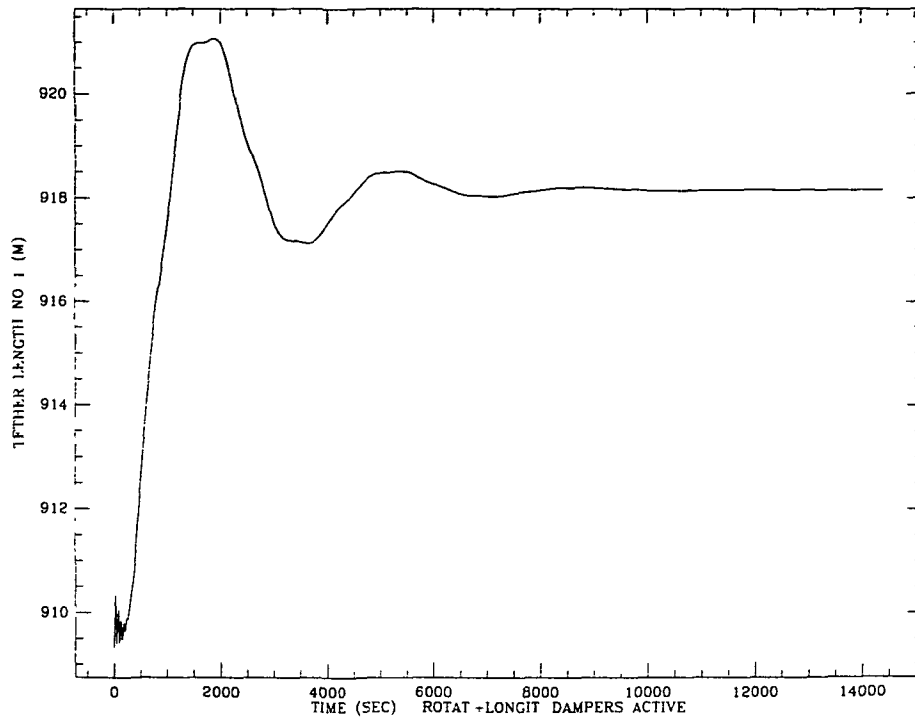
Figure 2.6.1 (m) and (n)

The initial conditions of this deployment maneuver are an in-plane attitude of  $30^\circ$  with respect to the local vertical and an initial alignment error of the three masses ( $\epsilon$ ) of 0.05 m. The dynamic response, however, does not differ significantly from a qualitative standpoint for varying values of the above mentioned parameters. Figure (a) and Figure (b) show the tether length and tether speed respectively of tether #1 vs. time. The same quantities for tether #2 can be obtained from those of tether #1 by scaling them up by a factor of 10. The deployment is performed in approximately 3 hours. This value however is affected by the initial tether length and is therefore eventually affected by the position of the reeling system on the Space Station. More important is the initial tether speed which must be as close as possible to the initial design speed, according to the law  $\dot{l}_I = \alpha l_I$ , in order to avoid tether slackening. In Figure (b) the different phases of the deployment control law are evident: the rotational damper-on results in the ripple on the plot at approximately 5500 sec, while the transition law-off results in the second ripple at 7500 sec. Figure (c) and Figure (d) show the tether #1 elastic stretch and longitudinal damper's length respectively vs. time. Here again it must be pointed out that the system should start the deployment with its natural tether stretch: an overstretch or an understretch induces longitudinal oscillations and reduces the margin for positive tension in the tether. It is also interesting to note the strong coupling between the elastic stretch and the longitudinal damper's length, as well as the capability of the system to damp out longitudinal oscillations as shown by the ripple around 8000 sec. This capability will be shown more clearly in the next subsection. Figure (e) shows the in-plane angle ( $\theta$ ) vs. time. Note that the acceleration phase of deployment is designed for a constant in-plane angle. Figure (f) is the phase plane  $\theta-\dot{\theta}$  and clearly shows the effectiveness of the rotational damper in damping out the attitude libration of the constellation. Figure (g) shows the tether tension for tether #1 which

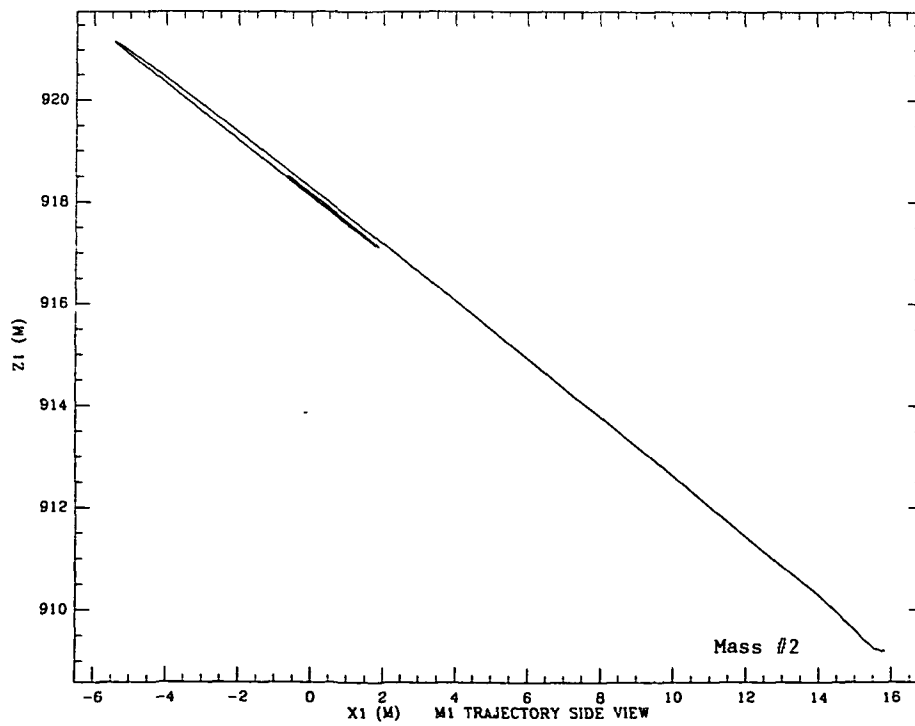
is approximately equal to that for tether #2. The tension is proportional to the tether elastic stretch (Figure c). Figure (h) shows the side-view of the trajectory of mass #1 (Space Station) with respect to the system center of mass. Mass #3 (the ballast) follows a specular trajectory scaled up by a factor 10. Mass #2 (the micro-g facility) remains very close to the system c.m. throughout the deployment maneuver. Figure (i) is the lateral displacement ( $\epsilon$ ) of mass #2 vs. time. When the rotational/transverse damper goes on at 5500 sec this oscillation begins to be damped out. Figure (l) is the phase plane  $\epsilon-\dot{\epsilon}$ . The damping of  $\epsilon$  is less effective than that of the in-plane angle  $\theta$  because the rotational/transverse damper is tuned to the in-plane oscillation. By using a control law like (2.3.5) instead of the simplified (2.3.6), that is, by using a multi-frequency damping technique, the damping of the transverse oscillation can be further improved. Finally Figure (m) and (n) give the horizontal (along the local horizon) and vertical components respectively of the acceleration at the micro-g facility vs. time. It is clear from these figures that the initial values of the acceleration due to the transverse oscillations of the system and the transient oscillations due to snapping of the tethers during transitions in the deployment control law are damped out very effectively by the various dampers. We shall return to this topic again in the next subsection which deals with modal vibrations damping during station-keeping.

## 2.7 Computer Simulation Of The Station-Keeping Phase

The effectiveness of the dampers during station-keeping is shown in the following set of plots. These plots have been obtained by simulating the dynamic response of the constellation during a station-keeping phase under the following initial conditions. The simulation begins with a tether length for tether #1 equal to 909 m and for tether #2 equal to 9090 m; the initial in-plane angle is  $1^\circ$  while the initial lateral deflection of mass #2 is 0.10 m. Figure 2.7.1(a) shows the tether length for tether #1 vs. time while Figure (b) is the side view of mass #1 trajectory. Figure (c) shows the tether's elastic stretch vs. time. Both these quantities are referred to tether #1: tether #2 has a qualitatively similar behavior. Figure (e) shows the in-plane angle vs. time and Figure (f) is the phase plane  $\theta-\dot{\theta}$ . Figure (g) shows the lateral deflection ( $\epsilon$ ) of mass #2 (the micro-g platform) vs. time and Figure (h) is the phase plane  $\epsilon-\dot{\epsilon}$ . The saw-teeth-like shape of this plot, near the beginning of the simulation, is due to an unsufficiently small plotting step and therefore it has no dynamic meaning. It is evident from these plots that any initial perturbations of the constellation are abated very effectively by the dampers. The final result is shown in Figure (i) and (l) which give the horizontal and vertical component respectively of the acceleration at mass #2 vs. time. The maximum accelerations at the end of this simulation are much smaller than  $10^{-8}g$ . This last point must not be misinterpreted: it means only that the system can effectively abate transient vibrations while the steady state acceleration level at mass #2 will depend upon the external steady state perturbations. These perturbations are not simulated in this analysis which deals with the transient response of the three-mass constellation.

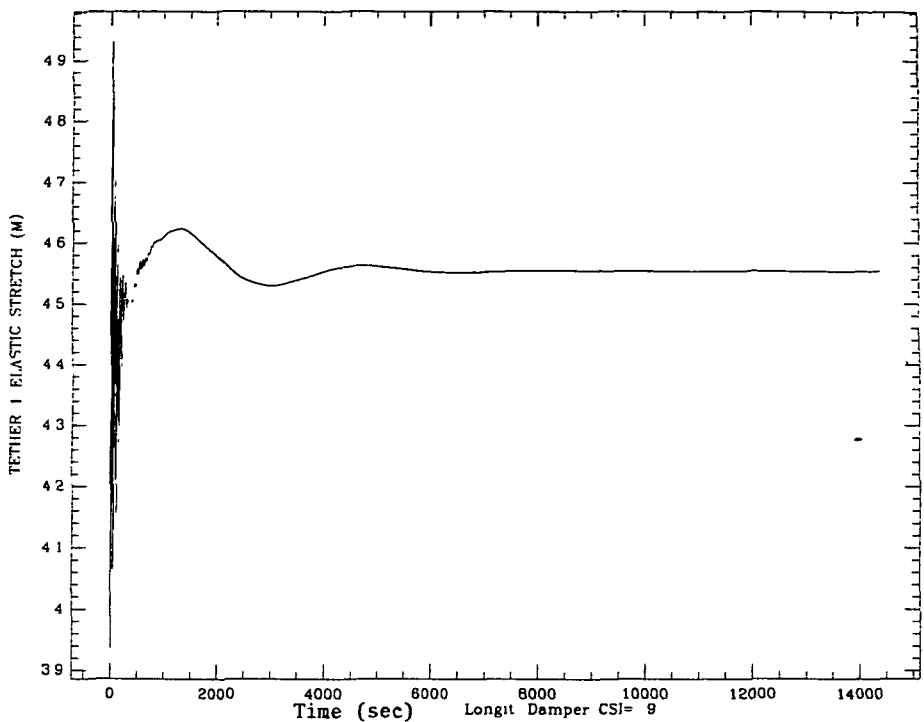


(a)

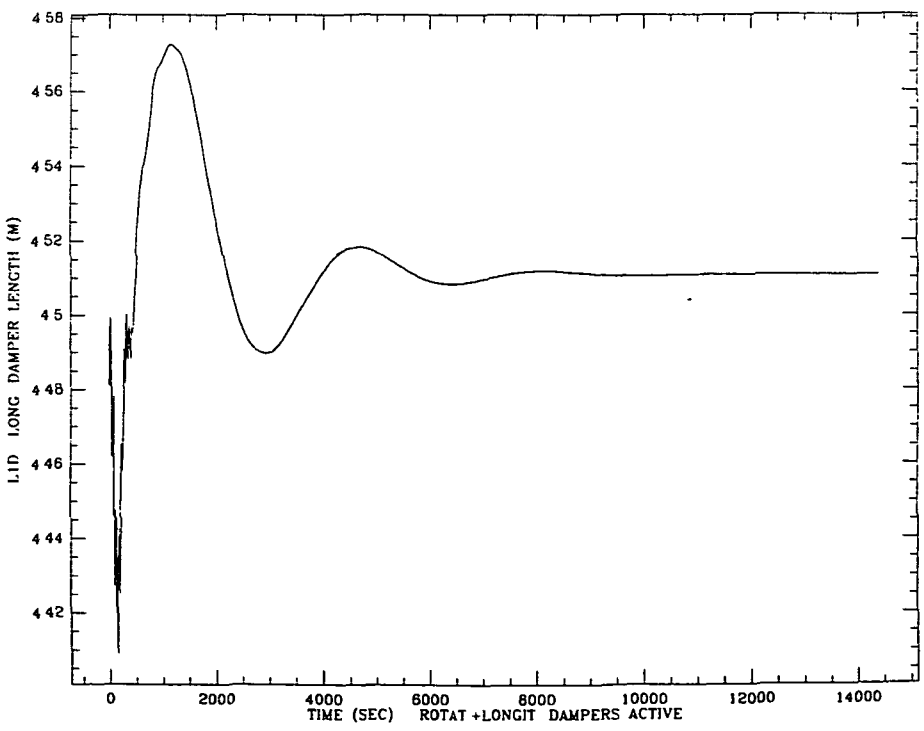


(b)

Figure 2.7.1 (a) and (b)

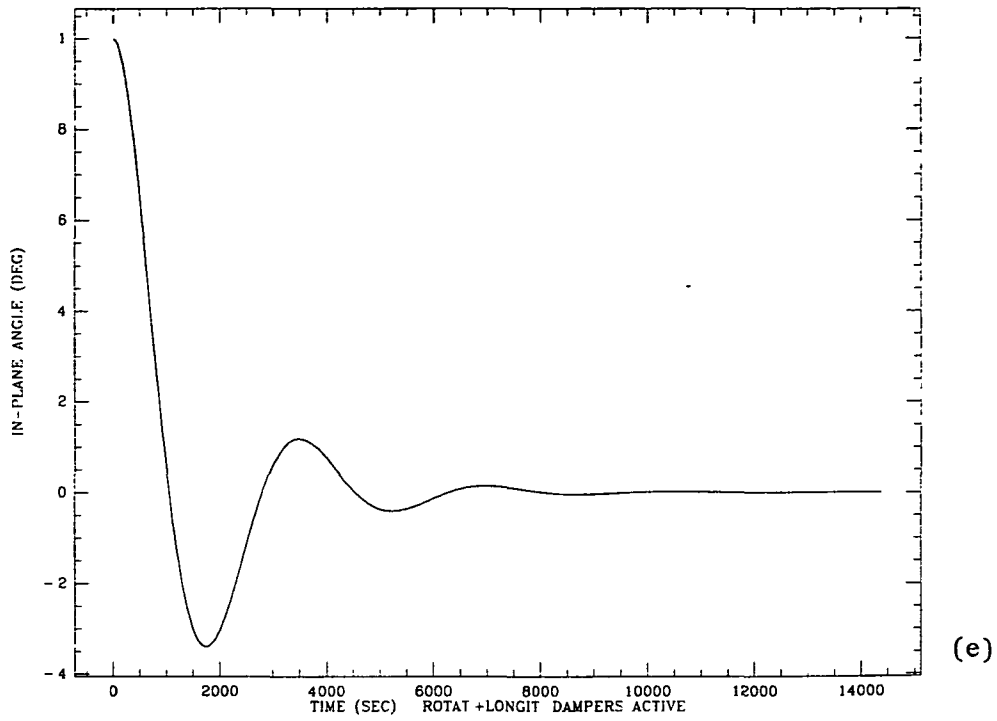


(c)

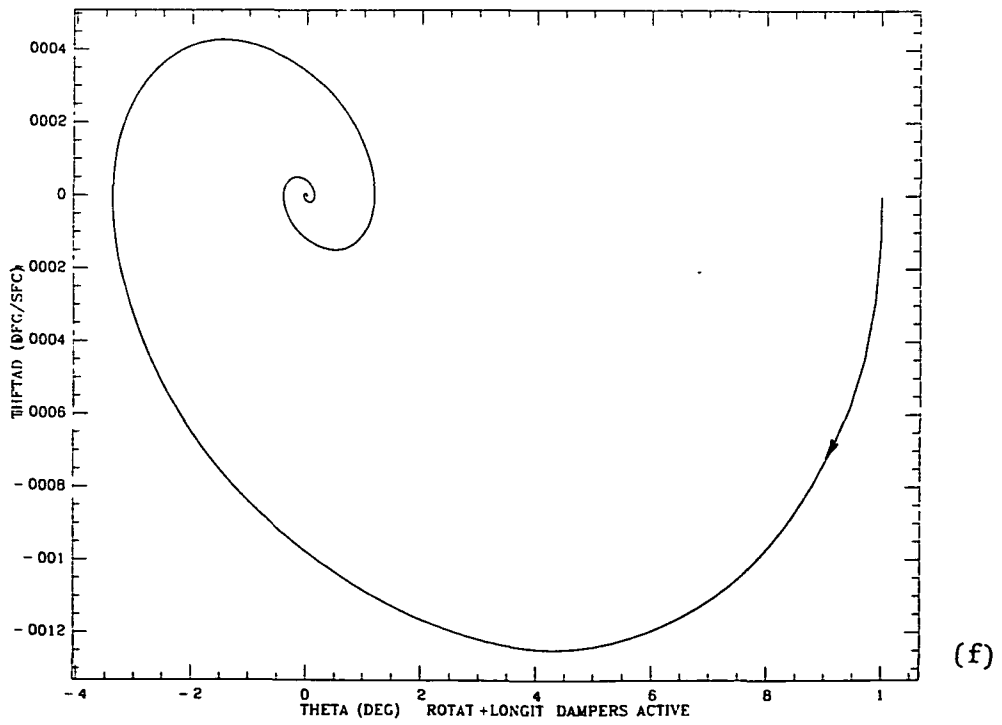


(d)

Figure 2.7.1 (c) and (d)

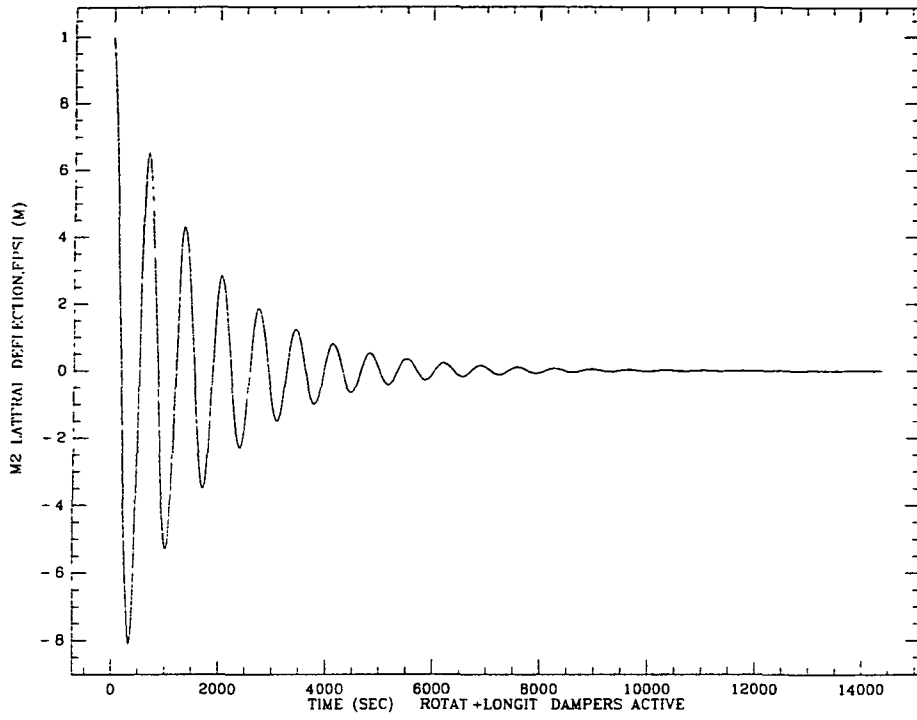


(e)

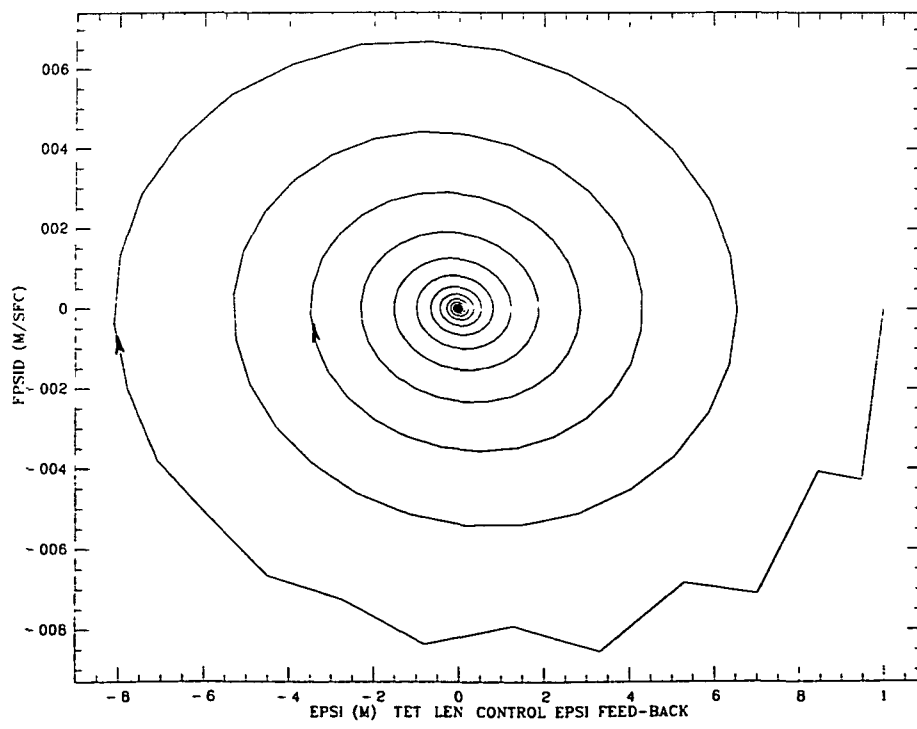


(f)

Figure 2.7.1 (e) and (f)



(g)



(h)

Figure 2.7.1 (g) and (h)

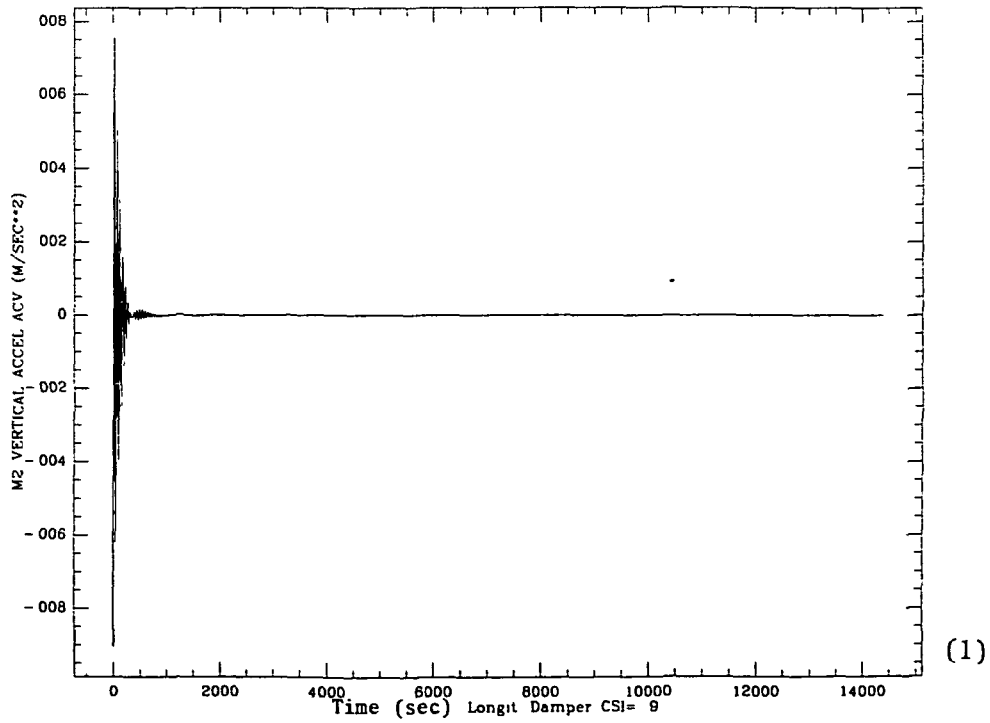
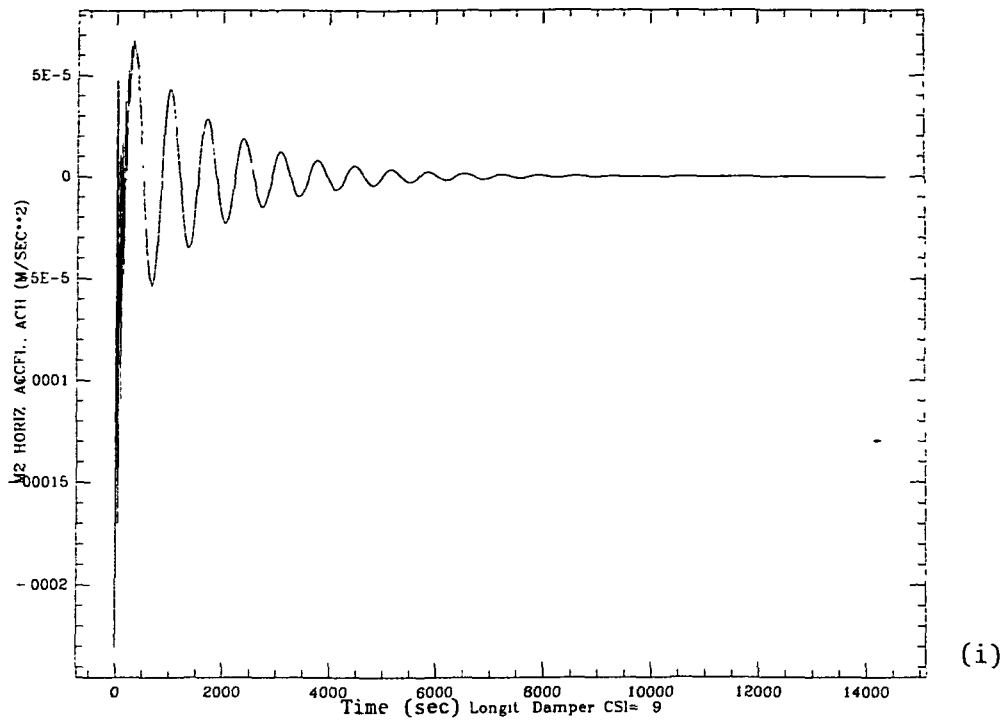


Figure 2.7.1 (i) and (1)

## 2.8 Concluding Remarks

Passive dampers for tethers' longitudinal oscillations have been added to the system with elastic tethers. Active control of rotational/transverse oscillations have been also added to the constellation. A new deployment strategy which drives the system to a steady state condition in approximately 3 hours has been devised. The initial part of deployment with elastic tethers, however, requires a more detailed investigation; as a result of such investigation the deployment duration may increase depending upon the minimum separation length of the end masses at the start of deployment. The dampers have been designed to provide an effective damping of the longitudinal, libratory and transverse oscillations of the system. The effectiveness of the dampers has been proven by computer simulations of the deployment and station-keeping phase. The damping of the modal vibrations can be further improved by multi-frequency active damping.

## 3.0 PROBLEMS ENCOUNTERED DURING REPORTING PERIOD

None

#### 4.0 ACTIVITY PLANNED FOR THE NEXT REPORTING PERIOD

During the next reporting period we will analyze the dynamics of three-mass constellations when the middle mass travels along the tether. Stability constraints and appropriate control laws will be sought. The investigation of the dynamics of a five-mass system, vertically oriented, attached to the Shuttle will also be initiated. This system potentially could be used as a scientific platform for measuring geophysical gradients.